Reflection and diffraction of atomic de Broglie waves by an evanescent laser wave

R. Deutschmann, W. Ertmer, and H. Wallis
Institut für Angewandte Physik der Universität Bonn, Wegelerstraße 8, D-5300 Bonn, Germany
(Received 3 August 1992)

The diffraction theory of a reflection grating for atoms based on a standing light wave is developed in a particular dressed-state approximation. The basis states take into account internal and external atomic degrees of freedom simultaneously and correspond to diffraction orders in the asymptotic region. In this basis the atom is described as an effective multilevel system. In an adiabatic approximation for the motion perpendicular to the grating, these levels serve as position-dependent potentials. An incoming de Broglie wave is coupled to higher diffraction orders by nonadiabatic transitions near avoided crossings of the potentials. Numerical results confirm the qualitative predictions following from the physical picture of the diffraction process and lead to an improved description of experiments.

PACS number(s): 32.80.Pj, 42.50.−p

I. INTRODUCTION

The diffraction of atomic de Broglie waves by material [1] or optical [2,3] structures has recently received considerable interest within the emerging field of atomic optics and interferometry. Atomic interferometry holds great promises to contribute to the realization of gedanken experiments concerning fundamental properties of quantum systems. Among these are the process of measurement or the distinction of dynamic, geometric, and topologic phases in the evolution of quantum systems.

A device of great practical importance for atomic interferometry but also intrinsic interest is the atomic reflection grating. Atomic reflection by a running evanescent laser wave is achieved through the potential barrier induced by the steep intensity gradient of the evanescent light [4,5]. Recently, also grating reflection by a standing evanescent light wave has been investigated theoretically [6] and experimentally [7]. Theoretically, a light force reflection grating poses several unusual problems. The motion perpendicular to the diffraction grating can no longer be eliminated in a constant motion approximation which has been applicable in all previous calculations of atomic diffraction by light, rendering a one-dimensional problem. By contrast, the slowing down and reversal of the atomic motion perpendicular to the mirror is essential for the light force reflection grating and the problem remains *necessarily* two dimensional. In this article we explain and predict the operation of the diffraction grating in a position-dependent basis of states which takes into account the coupling of momentum states by the standing light wave and the variation of this coupling with the exponentially decaying light intensity. Asymptotically, each considered momentum state corresponds to a diffraction order. Different orders are populated via the mixing of the momentum states in the interaction region. Our picture allows accurate calculations of diffraction patterns. It also introduces valuable insight in interference effects in the diffraction pattern with varying energy.

All calculations are done within some standard assumptions: First, our model system is a two-level atom interacting with a classical electromagnetic field in the rotating-wave approximation. Second, the basic phenomena are studied, neglecting spontaneous emission. This coherent regime is the important one for a successful operation of the reflection grating.

The structure of the paper is as follows: In Sec. II we outline the situation of atomic reflection by a running evanescent wave. For the running wave situation, the separation of the two-dimensional Schrödinger equation and a transformation to momentum representation for the motion parallel to the mirror (Sec. II A) gives back a simple one-dimensional picture. Using the dressed-state picture (Sec. II C) we discuss the reflection probabilites of the mirror for dressed-state de Broglie waves (Sec. II D). In Sec. III the diffraction grating formed by a standing evanescent laser wave is investigated. Solutions of the stationary Schrödinger equation (Sec. III A) are constructed starting from dressed states for the coupled momentum eigenstates (Sec. III B). Characteristic phenomena of the atomic motion in the dressed-state quasipotentials are described in Sec. III C, and our numerical predictions for the operation of the reflection grating are presented in Sec. IV. Our algorithms to compute nonadiabatic transitions in the running wave case and to construct the diffracted beam patterns are given in two appendixes.

II. REFLECTION BY AN EVANESCENT RUNNING WAVE

In this section the reflection of a two-level atom by a strong intensity gradient is considered. It serves to explain the idea of reflection by adiabatic motion in a quasipotential. The internal and external state is described by a (Schrödinger) spinor wave function, allowing for one ground state and one excited state.

A. Stationary Schrödinger equation

With the assumptions given in the Introduction, the Hamiltonian for the two-dimensional reflection of atoms by an evanescent light field reads

$$\hat{H} = \frac{-\hbar^2}{2m}\left(\frac{\partial^2}{\partial x^2} + \frac{\partial^2}{\partial y^2}\right) + \hat{H}_a - \hat{\boldsymbol{\mu}} \cdot \boldsymbol{\mathcal{E}}(x,y,t) \tag{2.1}$$

where the internal energy and the atom-laser coupling matrices read

$$\hat{H}_a = \begin{pmatrix} \varepsilon_e & 0 \\ 0 & \varepsilon_g \end{pmatrix}, \tag{2.2}$$

$$\hat{\boldsymbol{\mu}} \cdot \boldsymbol{\mathcal{E}}(x,y,t) = \begin{pmatrix} 0 & \mu\mathcal{E}(x,y,t) \\ \mu\mathcal{E}(x,y,t) & 0 \end{pmatrix} . \tag{2.3}$$

ε_e and ε_g denote the internal energy of the excited state and the ground state. $\boldsymbol{\mathcal{E}}(x,y,t)$ denotes the real electric field of the evanescent running wave of frequency ω for s polarization and $y \geq 0$

$$\boldsymbol{\mathcal{E}}(x,y,t) = \frac{1}{2}\left\{\mathcal{E}(x,y)\ \exp(-i\omega t) + \text{c.c.}\right\}\mathbf{e}_z\ . \tag{2.4}$$

The position-dependent amplitude is given by

$$\mathcal{E}(x,y) = \mathcal{E}_0 \exp(-qy)\exp(iQx), \quad y \geq 0 \tag{2.5}$$

with q taking into account the exponential decrease along the y direction (perpendicular to the surface; see Fig. 1) and Q denoting the x component of the wave number vector (parallel to the surface). $\mu \equiv \langle \mathbf{e}_z \cdot \boldsymbol{\mu} \rangle$ denotes the induced dipole moment of the transition and m the mass of the atom. The wave-vector components q and Q are related to the refractive index n of the medium which carries the evanescent wave and to the angle of incidence ϑ of the totally reflected laser wave by

$$q = k_0\sqrt{n^2\sin^2\vartheta - 1}, \qquad Q = k_0 n \sin\vartheta, \tag{2.6}$$

where k_0 is the vacuum wave vector of the light. The simple expressions (2.4) and (2.5) for the electric field are valid for s polarization (parallel to the surface, perpendicular to the plane of total internal reflection). Because of translational invariance with respect to the z direction the Hamiltonian acts on the two-dimensional spinor wave function $(\psi_e(x,y,t), \psi_g(x,y,t))^T$.

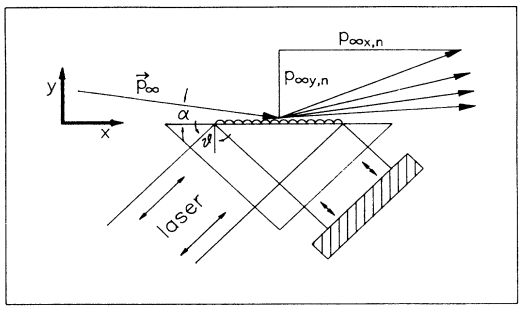

FIG. 1. Principle of diffraction: the evanescent standing wave is prepared by total internal reflection. Incoming and diffracted plane de Broglie waves are coupled by coherent momentum transfer parallel to the surface as given by $p_{\infty x,n} = p_{\infty x} + n\hbar Q$. Here $p_{\infty x}$ is the x component of the incoming momentum $\mathbf{p}_\infty$, n is the diffraction order, and Q is the x component of the light wave vector. The perpendicular momentum $p_{\infty y,n}$ is given by Eq. (3.2). α denotes the angle of grazing incidence of the atomic de Broglie wave, ϑ the angle of total internal reflection of the laser beam.

The transformation into the interaction picture in connection with the rotating-wave approximation eliminates rapidly varying terms, and the internal energy difference is replaced by the detuning

$$\Delta \equiv \omega - \frac{1}{\hbar}(\varepsilon_e - \varepsilon_g)\ . \tag{2.7}$$

Here and in the following sections the motion parallel to the surface (along the x axis) is treated in the momentum representation whereas the orthogonal component (along the y axis) is treated in the position representation. The stationary Schrödinger equation takes the form

$$E\begin{pmatrix} \phi_e(p_x+\hbar Q, y) \\ \phi_g(p_x, y) \end{pmatrix} = \begin{pmatrix} -\frac{\hbar^2}{2m}\frac{d^2}{dy^2} + \frac{(p_x+\hbar Q)^2}{2m} - \hbar\Delta & -\frac{1}{2}\mu\mathcal{E}_0\exp(-qy) \\ -\frac{1}{2}\mu\mathcal{E}_0\exp(-qy) & -\frac{\hbar^2}{2m}\frac{d^2}{dy^2} + \frac{p_x^2}{2m} \end{pmatrix}\begin{pmatrix} \phi_e(p_x+\hbar Q, y) \\ \phi_g(p_x, y) \end{pmatrix} . \tag{2.8}$$

As p_x appears solely as a parameter in this equation the x component $p_{\infty x}$ of the initial momentum $\mathbf{p}_\infty$ is conserved. This reflects the well known fact that a running laser wave couples a closed two-state family in momentum space, and the system behaves as a real two-level system for given momentum p_x. Obviously the quantity

$$T_{\infty y} \equiv E - \frac{p_{\infty x}^2}{2m} \tag{2.9}$$

is the conserved energy in a reference frame moving with the velocity $\frac{p_{\infty x}}{m}\mathbf{e}_x$. In this frame it equals the kinetic energy $T_{\infty y} = p_{\infty y}^2/(2m)$ of an atom moving along the y direction in the ground state and in the asymptotic region. If the atom, initially being in the ground state, is reflected from the mirror in the excited state, the kinetic energy has to compensate for the changed internal energy. Thus one obtains different y components of the atomic momentum in the asymptotic region depending on the internal state

$$p_{\infty y}^{(g)} = \sqrt{2mT_{\infty y}}, \qquad p_{\infty y}^{(e)} = \sqrt{2m(T_{\infty y} + \hbar\Delta_{\text{eff}})}, \tag{2.10}$$

where an effective detuning is defined to include the Doppler shift Δ_D and the recoil shift Δ_R:

$$\Delta_{\text{eff}} = \Delta - \Delta_D - \Delta_R \tag{2.11}$$

with

$$\Delta_D \equiv Q\frac{p_{\infty x}}{m} \qquad \Delta_R \equiv \frac{\hbar Q^2}{2m} . \tag{2.12}$$

Defining further the on-resonance Rabi frequency

$$\Omega(y) \equiv \frac{\mu \mathcal{E}_0}{\hbar} \exp(-qy), \tag{2.13}$$

we arrive at a more compact notation of the Schrödinger equation

$$E\,\Phi(y) = \left\{-\frac{\hbar^2}{2m}\frac{d^2}{dy^2} + \hat{H}_{\rm int}(y)\right\}\Phi(y), \tag{2.14}$$

where (with momentum arguments suppressed)

$$\Phi(y) = \begin{pmatrix}\phi_e(y)\\ \phi_g(y)\end{pmatrix} \tag{2.15}$$

is the state vector for given p_x and

$$\hat{H}_{\rm int}(y) = -\begin{pmatrix}\hbar\Delta_{\rm eff} & \frac{\hbar}{2}\Omega(y)\\ \frac{\hbar}{2}\Omega(y) & 0\end{pmatrix} \tag{2.16}$$

is the y-dependent internal energy of the coupled system of atom and running evanescent laser wave.

B. Dimensionless versus physical parameters

Before discussing numerical examples in the following sections, we establish suitable units for physical parameters. It is most convenient to express all energies in units of

$$\hbar\Delta_q \equiv \frac{(\hbar q)^2}{2m} \tag{2.17}$$

(the recoil shift for the imaginary wave-vector component q of the evanescent wave), which yields the Schrödinger equation dimensionless. Two different sets of parameters determine equivalent dynamics of the system if corresponding energy parameters have the same value in units of $\hbar\Delta_q$. Concerning the unit Δ_q, different atomic masses m and m' may be compensated for by q and q' with $\frac{q}{q'} = \sqrt{\frac{m'}{m}}$. q may be varied by adjusting the angle of internal reflection ϑ [Eq. (2.6)].

Physical parameters that correspond to the dimensionless parameters (used in the discussions below and in the figure captions) depend on the given experimental situation. We consider an evanescent wave which is prepared by a light wave with vacuum wavelength $\lambda = 640$ nm under an angle of internal reflection of $\vartheta = 45°$ and a refractive index of the medium of $n = 1.56$. The atomic mass m is that of ^{20}Ne. From these data one obtains the conversion factors given in Table I. We assume the incoming de Broglie wave to be an ideal plane wave.

C. Schrödinger equation in the adiabatic basis: quasipotentials

A convenient way to obtain the solutions of the Schrödinger equation consists in diagonalizing the y-dependent internal part (2.16) and to transform to the local eigenvector basis, also called the adiabatic or dressed basis [2, 8]. The adiabatic energy levels are given by the eigenvalues $W_{1,2}(y)$ of (2.16) (see Fig. 2)

$$W_{1,2}(y) = -\frac{\hbar}{2}[\Delta_{\rm eff} \pm \Omega_R(y)], \tag{2.18}$$

where

$$\Omega_R(y) \equiv \sqrt{\Delta_{\rm eff}^2 + \Omega^2(y)} . \tag{2.19}$$

The basis of eigenstates $\{e_1(y), e_2(y)\}$ of $H_{\rm int}(y)$ may be written as

$$e_1(y) = \begin{pmatrix}u(y)\\ v(y)\end{pmatrix}, \qquad e_2(y) = \begin{pmatrix}-v(y)\\ u(y)\end{pmatrix} \tag{2.20}$$

where

$$u(y) = \left(\frac{\Omega_R(y) + \Delta_{\rm eff}}{2\Omega_R(y)}\right)^{1/2},$$
$$v(y) = \left(\frac{\Omega_R(y) - \Delta_{\rm eff}}{2\Omega_R(y)}\right)^{1/2}. \tag{2.21}$$

For $\Delta_{\rm eff} > 0$ the adiabatic state e_1 approaches the excited state in the limit of vanishing Rabi frequency, and e_2 approaches the ground state; for $\Delta_{\rm eff} < 0$ it is vice versa. Per definition, it is always the energy level W_2 which forms the potential barrier. The internal state spinor of a pointlike atom will adiabatically follow the quasienergy levels $W_{1,2}$, if the internal precession frequency $\Omega_R(y)$ is large compared to the reciprocal rise time of the electric-field amplitude $T_{\rm rise}^{-1} \equiv \Omega^{-1}(\frac{p_y}{m})(\frac{d\Omega}{dy})$. As $T_{\rm rise}^{-1}$ is of the order of the Doppler shift $q(\frac{p_y}{m})$ for the y component of the velocity, such an assumption seems reasonable since large values of Ω_R are necessary for reflection anyway. For appreciable detuning Δ, usually chosen for atomic reflection, the Rabi frequency $\Omega_R(y)$ is much larger than $T_{\rm rise}^{-1}$ along the *whole* y axis. If, however, the detuning is too small to yield Ω_R much larger than $T_{\rm rise}^{-1}$ in the

TABLE I. Relations between dimensionless parameters and physical parameters as explained in Sec. II B: for a laser wavelength $\lambda = 640$ nm, an angle of internal reflection of $\vartheta = 45°$, a refractive index of the medium $n = 1.56$, and the atomic mass m of ^{20}Ne, the energy unit $\hbar\Delta_q$ [Eq. (2.17)] corresponds to the following cycle frequencies and atomic velocities.

Experimental parameter	Letter	Conversion to frequency unit Δ_q	First reference
Rabi frequency	$\Omega, \Omega_\pm$	$19.0 \times 10^4 \Delta_q = 2\pi \times 1$ GHz	Eq. (2.13)
Detuning	$\Delta, \Delta_{\rm eff}$		Eq. (2.7)
Perpendicular kinetic energy	$T_{\infty y}$	$9600\,\frac{\hbar\Delta_q}{m} = (1\text{m/s})^2$	Eq. (2.9)
Longitudinal Doppler shift	Δ_D	$327\frac{\Delta_q}{Q} = 1$m/s	Eq. (2.12)

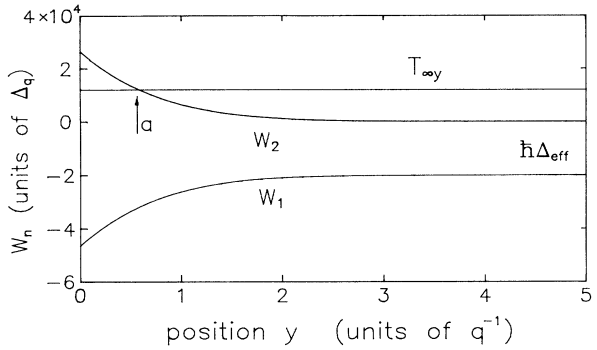

FIG. 2. Quasipotentials W_1 and W_2 Eq. (2.18) for the dimensionless parameters $\Omega(0) = 7 \times 10^4 \Delta_q$, $\Delta_{\text{eff}} = 2 \times 10^4 \Delta_q$. Here $\hbar\Delta_q \equiv \frac{(\hbar q)^2}{2m}$ is used as the energy unit, for physical parameters, see Table I. For $T_{\infty y} = 1.2 \times 10^4 \hbar\Delta_q$ ($p_{\infty y}/m = 1.6$ m/s) a classical turning point a exists. For positive detuning, ground-state atoms, incoming in W_2, are reflected at the classical turning point a whereas excited state atoms, incoming in W_1, reach the surface.

asymptotic region, nonadiabatic effects arise. They are explicitly treated in Sec. II D and Appendix A.

The solution of the total Schrödinger equation may now be found by expansion in the adiabatic basis

$$\Phi(y) = \alpha_1(y)e_1(y) + \alpha_2(y)e_2(y). \tag{2.22}$$

In the adiabatic approximation the resulting derivatives of the basis vectors are neglected similar to the Born-Oppenheimer approximation. Equation (2.14) then decouples into two scalar equations for the coefficients α_n, $n = 1, 2$,

$$T_{\infty y}\, \alpha_n(y) = \left(-\frac{\hbar^2}{2m}\frac{d^2}{dy^2} + W_n(y) \right) \alpha_n(y)\,. \tag{2.23}$$

Each of the equations (2.23) describes the center-of-mass wave function $\alpha_n(y)$ of an atom being in a position-dependent superposition state $e_1(y)$ or $e_2(y)$ given by (2.20). As both solutions belong to the same energy, any linear combination $c_1\,\alpha_1 e_1 + c_2\,\alpha_2 e_2$ of them forms another solution (c_1, c_2 complex numbers). Physical solutions are singled out by imposing boundary conditions at $y = 0$ and ∞, as done in Sec. II D.

D. Reflection of dressed state de Broglie waves

The application of the evanescent running wave as a mirror in atomic cavities requires an highly efficient reflection of the ground-state wave [9, 10]. This is achieved by choosing the detuning positive. An incoming wave in the atomic ground state is described by an incoming part of α_2 in the repulsive potential W_2 and zero amplitude in the attractive potential W_1. If the energy $T_{\infty y}$ is sufficiently small compared to the maximum value of $W_2(y = 0)$ it will be completely reflected (Fig. 2). By contrast, an incoming excited-state wave is described by the incoming part of α_1 in the attractive potential W_1. Such a de Broglie wave will always reach the surface and atoms will be adsorbed or incoherently scattered by the surface.

The light field has to be strong enough to provide a turning point of the potential $W_2(y)$ [Eq. (2.18)]. The reflection of the incoming wave α_2 is described in the WKB approximation [11]. In the classical allowed region $y > a$ near the turning point a we obtain a standing wave

$$\alpha_2(y) = \frac{1}{\sqrt{p_2(y)}}\, 2\cos\left\{ \frac{1}{\hbar}\int_a^y p_2(y')\,dy' - \frac{\pi}{4} \right\}, \tag{2.24}$$

where $p_2(y) = \sqrt{2m[T_{\infty y} - W_2(y)]}$ is the quasiclassical momentum. In the classical forbidden region $0 < y < a$ the exponential decaying solution reads

$$\alpha_2(y) = \frac{1}{\sqrt{\rho(y)}}\, \exp\left\{ \frac{1}{\hbar}\int_a^y \rho(y')\,dy' \right\} \tag{2.25}$$

with

$$\rho(y) = \sqrt{-2m[T_{\infty y} - W_2(y)]}\,. \tag{2.26}$$

An adiabatic stationary solution of the Schrödinger equation for an incoming ground-state wave is thus determined to be a pure reflected α_2 wave.

Obviously there exist three possible loss mechanisms which reduce this reflectivity: (a) tunneling of the de Broglie wave across the potential barrier, (b) nonadiabatic transitions from the incoming wave α_2 into the nonreflecting potential W_1, and (c) mixing of both states due to spontaneous emission.

(a) The loss of ground-state atoms due to tunneling of the amplitude of the repelled state through the potential barrier W_2 is estimated by the probability current of the WKB solution at $y = 0$. Using Eq. (2.26) and

$$\tau \equiv \frac{1}{\hbar}\int_0^a \rho(y')\,dy' \tag{2.27}$$

we obtain the loss due to tunneling as probability per reflection

$$L_T = |\exp(-\tau)|^2 = \exp(-2\tau)\,. \tag{2.28}$$

(b) A second loss mechanism is given in this representation by nonadiabatic transitions from the repelling state to the attractive state. These nonadiabatic transitions are strong for small detuning due to the near degeneracy of W_1 and W_2 in the asymptotic region which indicates a strong mixing of the adiabatic eigenvectors. This mixing results from the derivatives of the eigenvectors (2.20) which are neglected in the adiabatic approximation (2.23). Here we treat them as an additional perturbation $\hat{H}_{\text{NA}}$ of the total Hamiltonian

$$\hat{H} = \hat{H}_A + \hat{H}_{\text{NA}} \tag{2.29}$$

which causes nonadiabatic transitions. $\hat{H}_A$ is given by the right-hand side of (2.23). $\hat{H}_{\text{NA}}$ is given by

$$\hat{H}_{\mathrm{NA}} = -\frac{\hbar^2}{2m}\begin{pmatrix} -\left(\frac{d\Theta}{dy}\right)^2 & -\left(\frac{d^2\Theta}{dy^2}\right) + 2\left(\frac{d\Theta}{dy}\right)\frac{d}{dy} \\ \left(\frac{d^2\Theta}{dy^2}\right) - 2\left(\frac{d\Theta}{dy}\right)\frac{d}{dy} & -\left(\frac{d\Theta}{dy}\right)^2 \end{pmatrix}. \tag{2.30}$$

Here Θ denotes the angle by which the position-dependent basis of eigenvectors is rotated against the asymptotic basis [from (2.20) and (2.21)] $\tan(\Theta) = v/u$.

If an incoming wave is reflected by the repulsive potential W_2, the perturbation $\hat{H}_{\mathrm{NA}}$ provides a position-dependent source for waves in the potential W_1. This source is predominantly localized at a particular range in the positive y direction and disappears in those regions where either the wave function α_2 vanishes (negligible in $y = 0$) or the first and second derivative of Θ vanishes ($y \to \infty$). Thus the total nonadiabatic loss L_{NA} is given by the flux of the wave function in W_1 both incoming onto the surface as well as outgoing in the instable excited state. An explicit expression for the nonadiabatic loss L_{NA} is derived in Appendix A on the basis of the distorted-wave approximation.

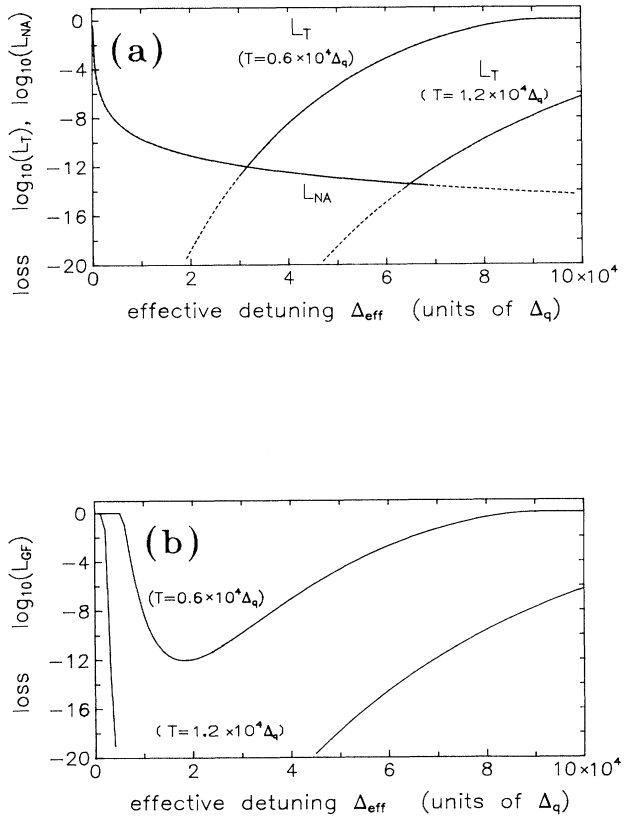

FIG. 3. Loss probability per reflection calculated for varying detuning and *fixed* Rabi frequency (logarithmic vertical axis): (a) L_T is the tunneling loss calculated for the adiabatic potential barrier W_2 for $\Omega(0) = 7 \times 10^4 \Delta_q$ and two values of the kinetic energy: $T_{\infty y} = 0.6 \times 10^4 \hbar\Delta_q$ ($p_{\infty y}/m = 1.1$ m/s) and $T_{\infty y} = 1.2 \times 10^4 \hbar\Delta_q$ ($p_{\infty y}/m = 1.6$ m/s). L_{NA} is the upper bound for nonadiabatic loss (see Appendix A), valid for both values of the kinetic energy. (b) Tunneling loss L_{GF} for the potential of the gradient force W_{GF} [Eq. (2.31)] for parameters as in (a) and $A = 1800\Delta_q$.

(c) The above results are to be compared with the loss L_{GF} calculated from Eqs. (2.26) and (2.27) for the potential barrier W_{GF} of the gradient force, taken from [4], instead of W_2:

$$W_{\mathrm{GF}}(y) = \frac{\hbar\Delta}{2}\ln\left\{1 + 2\frac{\Omega^2(y)}{A^2 + 4\Delta^2}\right\}. \tag{2.31}$$

Here A denotes the rate of spontaneous emission. In the dressed-state model spontaneous emission averages the forces due to the repulsive and the attractive dressed-state potential, with the weights of the dressed-state populations. According to the difference between these populations the gradient force W_{GF} vanishes as saturation increases. Thus in general the neglection of spontaneous emission severely modifies the prediction for the reflectivity. However, in the limit of large detuning the results for reflection by the gradient force potential and the adiabatic potential converge.

A comparison of the results for fixed Rabi frequency and varying detuning is given in Fig. 3. The deviation between the curves calculated for W_2 and W_{GF} is due to spontaneous transitions between the dressed states. Since the transition rate depends on the excited-state population, it decreases with decreasing saturation.

To minimize loss due to both nonadiabatic and spontaneous transitions the detuning might be increased as long as the repulsive potential barrier remains sufficiently high. The total loss of tunneling and nonadiabatic transitions $L_T + L_{\mathrm{NA}}$ can be driven safely below 10^{-10} for slow atoms with a y component of velocity (perpendicular to the surface) $v_y \lesssim 1$ m/s using conventional laser technology to produce the evanescent wave. Thus the laser-induced mirror is suitable to serve in atomic resonators.

III. DIFFRACTION

We now turn to the description of the atomic reflection grating which is created when the laser wave is retroflected into itself (see Fig. 1). The physical behavior of the system is governed by the combined action of diffraction and reflection. Whereas diffraction phenomena occur for the parallel component p_x of the momentum, the perpendicular component p_y introduces a smooth variation of the coupling strength from zero in the asymptotic region $y \to \infty$ to a certain maximum value at the surface.

In the case of the standing wave the idea of a potential barrier has to be generalized to allow for the different diffracted beams. However, the adiabatic potentials have

a much more complicated structure compared to Fig. 2 due to the possibility of infinite coherent momentum exchange with the standing laser field in the x direction. The coupling of the momentum channels results in a new feature of the quasipotentials, namely avoided crossings. These may cause nonadiabatic transitions transfering population to different diffraction orders. Their evaluation requires the solution for the perpendicular atomic motion in the y direction, which is done fully wave mechanically.

A. Stationary Schrödinger equation

The reflection grating is formed by adding an additional counterpropagating running wave (with amplitude $\mathcal{E}_-$) to the incoming evanescent wave (with amplitude $\mathcal{E}_+$). Thus we replace Eq. (2.5) by

$$\mathcal{E}(x,y) = \exp(-qy)\,\{\mathcal{E}_+ \exp(iQx) + \mathcal{E}_- \exp(-iQx)\}\,. \tag{3.1}$$

In the following, we consider an atom incoming in the ground state and in a momentum eigenstate with initial momentum $\mathbf{p}_\infty$. The spatial periodicity of the standing wave gives rise to a net momentum transfer in the x direction $n\hbar Q$ onto the atom, with n being an integer number which is *even* for atoms leaving in the ground state and *odd* for atoms leaving in the excited state. The x component of the atomic momentum in the nth diffraction order being $p_{\infty x} + n\hbar Q$, the asymptotic y component of the momentum is calculated from conservation of momentum and energy according to

$$p_{\infty y,n} = \pm\sqrt{2m(T_{\infty y} + \varepsilon_n\,\hbar\Delta - n\hbar\Delta_D - n^2\hbar\Delta_R)}, \tag{3.2}$$

using Δ_D and Δ_R from (2.12) and $\varepsilon_n \equiv \frac{1}{2}\{1-(-1)^n\}$, which gives 0 for even (ground-state) diffraction orders and 1 for odd (excited-state) orders. Note that the y component of the asymptotic momentum depends on the internal atomic state by the term $\varepsilon_n\hbar\Delta$ as well as on the x component of the momentum. The negative sign in Eq. (3.2) corresponds to the transmitted orders which are adsorbed. An infinite family of coherently coupled basis states for the internal and external degrees of freedom is conveniently defined using the notation

$$|n,y\rangle \equiv \begin{cases} |e, p_{\infty x} + n\hbar Q, y\rangle, & n \text{ odd} \\ |g, p_{\infty x} + n\hbar Q, y\rangle, & n \text{ even} \end{cases} \tag{3.3}$$

and

$$\phi_n(y) \equiv \langle\Phi|n,y\rangle\,. \tag{3.4}$$

The momentum-space representation for the x motion is reduced to the number n whereas the y motion remains to be treated in position space; the family momentum $p_{\infty x}$ is not changed by the coherent interaction. Using Eq. (3.4) and $T_{\infty y}$ from (2.9) the Schrödinger equation for $\phi_n(y)$ reads

$$\left(T_{\infty y} + \frac{\hbar^2}{2m}\frac{d^2}{dy^2}\right)\phi_n(y) = \sum_{n'} (\hat{H}_1(y))_{n,n'}\,\phi_{n'}(y), \tag{3.5}$$

where for fixed y the matrix $\hat{H}_1(y)$ is given by

$$\begin{aligned}(\hat{H}_1(y))_{n,n'} = {}& \delta_{n,n'}\,\hbar(-\varepsilon_n\Delta + n\Delta_D + n^2\Delta_R) \\ & + \frac{\hbar\Omega_+(y)}{2}\{(1-\varepsilon_n)\delta_{n,n'+1} + \varepsilon_n\delta_{n,n'-1}\} \\ & + \frac{\hbar\Omega_-(y)}{2}\{(1-\varepsilon_n)\delta_{n,n'-1} + \varepsilon_n\delta_{n,n'+1}\}\end{aligned} \tag{3.6}$$

with $\delta_{n,n'}$ denoting Kronecker's delta function and

$$\Omega_\pm(y) \equiv \frac{\mu\mathcal{E}_\pm}{\hbar}\exp(-qy)$$

the position-dependent Rabi frequencies. $\hat{H}_1(y)$ is a position-dependent effective Hamiltonian. Allowance for the discrete momentum exchange with the standing laser wave has turned the two-level atom into an effective multi-level system. Correspondingly, Eq. (3.5) resembles a multichannel Schrödinger equation for an inelastic collision problem.

From energy and momentum conservation one obtains the range of allowed numbers n corresponding to real values of $p_{\infty y,n}$

$$|2n\Delta_R + \Delta_D| \le \sqrt{4\Delta_R\left(\frac{T_{\infty y}}{\hbar} + \varepsilon_n\Delta\right) + \Delta_D^2}. \tag{3.7}$$

For vanishing coupling ($\Omega_+ = \Omega_- = 0$) the matrix (3.6) gives therefore a finite number of open channels.

The effective Hamiltonian (3.6) has been treated in various approximations previously and its eigenvectors have been determined by solving recurrence relations [12]. We remark that one can distinguish two types of $\Delta \neq 0$ resonances between momentum channels: the first one, termed Bragg resonance, occurs between asymptotic states of quantum number n and $-n$ and involves an exchange of an even number of photon momenta; the second one is inelastic and velocity tuned; neglecting the quadratic term $n^2\Delta_R$ its resonance condition for vanishing Stark shift reads

$$\Delta - n\Delta_D = 0, \quad n \text{ odd} \tag{3.8}$$

and they are called Doppleron resonances [13, 14]. Here we are interested in the limit of strong coupling, comparable to the energy-level spacing $\hbar\Delta_D$, such that a perturbative treatment of the resonances [14] is no longer sufficient.

B. Adiabatic quasipotentials and avoided crossings

The basic feature of our treatment is to use the eigenvalues $W_n(y)$ of the Hamiltonian $\hat{H}_1(y)$ (3.6) as position-dependent quasipotentials for a multilevel atom [Fig. 4(a)]. To compute these quasipotentials numerically, we use a suitably truncated effective Hamiltonian $\hat{H}_1$ [15].

In the asymptotic region the energy values coincide with the diagonal elements of $\hat{H}_1$. The energy values form a level sequence which is equidistant with the level spacing Δ_D up to the small shifts $n^2\hbar\Delta_R$, even $W_{2l}(y)$ and odd $W_{2l+1}(y)$ alternating with each other. Varying the detuning Δ shifts the sequence of the odd levels up or down with respect to the even levels which are independent of Δ. When approaching the surface $y = 0$ the light-induced coupling increases to its maximum value. As a consequence, all energy levels are y-dependently shifted, ground states $[W_{2l}(y)]$ are repelled from excited states $[W_{2l+1}(y)]$ and vice versa. For the purpose of reflection, this shift has to be larger than the component of the kinetic energy perpendicular to the surface $T_{\infty y}$. The

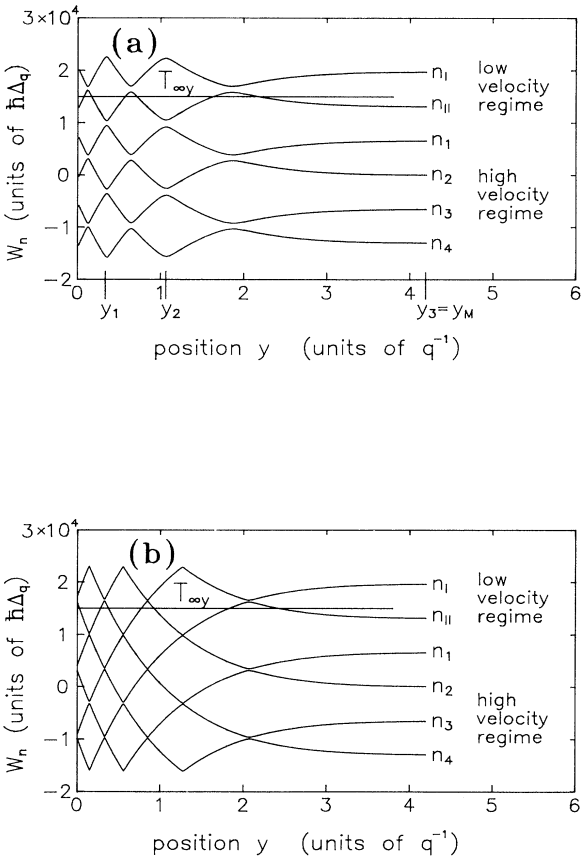

FIG. 4. Quasipotentials obtained as position-dependent eigenvalues of $\hat{H}_1(y)$ [Eq. (3.6)]: (a) Quasipotentials for the dimensionless parameters $\Omega_+(0) = 7 \times 10^4\Delta_q$, $\Omega_-(0) = 3\times10^4\Delta_q$, $\Delta = 1.3\times10^4\Delta_q$, $\Delta_D = 6520\Delta_q$, $\Delta_R = 5.6\Delta_q$, and $T_{\infty y} = 1.5\times10^4\hbar\Delta_q$. These parameters are chosen to optimize the even diffraction orders. They are further used in Figs. 7–9 and discussed in Sec. IV. Here $\Delta_q \equiv \frac{\hbar q^2}{2m}$; for physical parameters see Table I. The positions $y_m, m = 1,\ldots,3$, and y_M are defined in the discussion of Appendix B. (b) Quasipotentials for parameters as in (a) but for dominating running wave $\Omega_+(0) = 9 \times 10^4\Delta_q$, $\Omega_-(0) = 1 \times 10^4\Delta_q$. The energy separation in each avoided crossing is too small to be visible on this scale. Therefore the shown adiabatic (noncrossing) potentials almost coincide with the diabatic (crossing) potentials.

adiabatic approximation consists in replacing Eq. (3.5) by a number of single-channel Schrödinger equations for the scalar wave functions $\alpha_n(y)$:

$$-\frac{\hbar^2}{2m}\frac{d^2}{dy^2}\alpha_n(y) = [T_{\infty y} - W_n(y)]\,\alpha_n(y)\ . \tag{3.9}$$

As shown in Fig. 4(a) the adiabatic potentials $W_n(y)$ exhibit a characteristic structure of avoided level crossings. They play an important role in coupling different diffraction orders.

In the asymptotic region the sign of the slope of the quasipotentials $[dW_n(y)/dy]$ depends on its index n being even or odd and on the value of the detuning, e.g., for positive sign of the effective detuning (approximately given by $\Delta - \Delta_D$) even potentials (e.g., the zeroth order) are reflective. Passing an avoided crossing on the adiabatic curves, however, reverses the sign of the slope so that the adiabatic potentials are in general no longer strictly repulsive or attractive as in the case of the running wave.

On the other hand, diabatic curves [16] [refer to Fig. 4(b)] are either strictly repulsive or strictly attractive. We use the repulsive diabatic curves to determine the maximum number of nonvanishing diffraction orders. Reflected waves are expected in those asymptotic open channels that correspond to diabatic curves which are sufficiently shifted upwards to provide a turning point [Fig. 4(b)]. Increasing the energy $T_{\infty y}$ [Eq. (2.9)] by increasing the angle of grazing incidence α (Fig. 1) has two consequences. First, diffraction orders which are asymptotically forbidden, will become allowed. Second, diabatic potentials will lose reflectivity as the asymptotic kinetic energy exceeds the maximum light-induced shift of the diabatic curves. Thus the maximum asymptotic momentum $p_{\infty y}^{\max}$ of nonvanishing diffraction orders is defined by the condition that $(p_{\infty y}^{\max})^2/(2m)$ equals the maximum light shift. Consequently, the angles with the surface are confined to a limited interval

$$[0, \arctan(p_{\infty y}^{\max}/p_{\infty x})]\ . \tag{3.10}$$

This limitation will show up in the numerical results in Sec. IV.

C. Diffraction process in the multilevel approximation

In the following we discuss several features of the propagation of de Broglie waves in the quasipotentials leading to reflection of the incoming wave and to population of higher diffraction orders.

1. *Reflection barriers and transmission gaps*

Atoms will be reflected if at least part of the de Broglie wave encounters a classical turning point along its path to the surface. Unfortunately, in the adiabatic representation, for a given energy, there is at most one single adiabatic potential curve which provides classical turning points [Fig. 4(a)]. However, nonadiabatic transitions

enable an incoming atom to follow (preferably) repulsive diabatic curves by changing from one adiabatic curve to the next.

To establish the notation for the following discussion we first distinguish certain classes of adiabatic potentials [refer to Fig. 4(a)].

First, there is a pair of potential curves closest to a line of constant energy $E = T_{\infty y}$. One of these two potentials provides classical turning points and essentially determines the reflection. They are numbered $W_{n_{\rm I}} > W_{n_{\rm II}}$ and referred to as the *low-velocity regime* (Sec. III C 3). The kinetic energy of an atom in these potentials is too small to allow a semiclassical (e.g., WKB) treatment. Additionally, although $W_{n_{\rm I}}$ is at least partially forbidden, it affects the motion in $W_{n_{\rm II}}$. A full numerical calculation of the atomic dynamics in $W_{n_{\rm I}}$ and $W_{n_{\rm II}}$ is discussed in Appendix B 2.

Second, there are potentials which lie entirely below $W_{n_{\rm II}}$ and are in any case entirely allowed. They are numbered $W_{n_1} > W_{n_2} > W_{n_3} > \cdots$ and referred to as *high-velocity regime* (Sec. III C 2). These potentials can be considered to vary smoothly on the scale of the local de Broglie wavelength. Therefore a WKB treatment is justified. Semiclassical motion in these potentials is discussed in Appendix B 1.

Here and below, the indices $n = n_{\rm I}$, $n_{\rm II}$, and n_i denote the coherent momentum transfer $(p + n\hbar Q)$ of the asymptotic state n, whereas the indices I,II,i denote the ordering of the states with respect to energy.

Finally, there are potentials which lie above $W_{n_{\rm I}}$ and are in any case entirely forbidden (not shown in Fig. 4). Therefore they do not affect the motion in the low-velocity regime and in the high-velocity regime and are discussed in the following.

Of course it may happen that the line of constant energy $E = T_{\infty y}$ is entirely between $W_{n_{\rm I}}$ and $W_{n_{\rm II}}$ for some certain values of $T_{\infty y}$ [Fig. 5(a)]: i.e., an atom with this energy does not encounter any classical turning point. These energy gaps will show up in the energy dependence of the diffraction patterns (Sec. IV).

One of the advantages of the adiabatic representation of the problem is that physically motivated boundary conditions for the de Broglie wave propagation in each single channel can be defined. This is possible inasmuch as the eigenstates of the effective Hamiltonian $\hat{H}_1$ can be considered as decoupled (adiabatic approximation). Single-channel wave functions are thus definitely energetically allowed or forbidden in $y = 0$. We demand entirely incoming waves in $y = 0$ if the potential is allowed in $y = 0$. This corresponds to the assumption that the surface provides a perfect drain for incoming de Broglie waves (e.g., as a consequence of adsorption but no coherent reflection). On the other hand, energetically forbidden potentials in $y = 0$ lead to exponentially decreasing wave amplitudes because of tunneling.

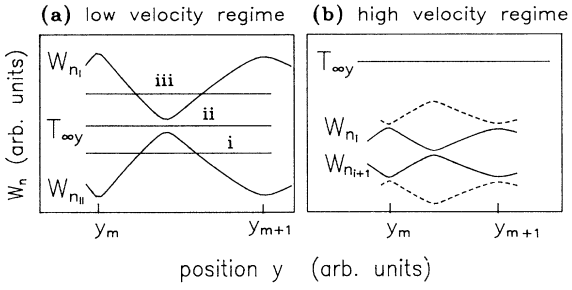

FIG. 5. (a) Quasipotentials $W_{n_{\rm I}}$ and $W_{n_{\rm II}}$ of the low velocity regime: The three different values of $T_{\infty y}$ lead to (i) barrier reflection, (ii) adiabatic overbarrier motion, and (iii) coupling to quasibound states. (b) Quasipotentials W_{n_i} and $W_{n_{i+1}}$ of the high-velocity regime: Note the much higher kinetic energy as compared to (a).

We turn now to the different formal treatment of the wave function in the lower potentials W_{n_i} and in $W_{n_{\rm I}}$, $W_{n_{\rm II}}$.

2. *High-velocity regime*

In the lower potentials the kinetic energy $T_{\infty y} - W_{n_i}(y)$ (and the velocity) is sufficently large to permit a semiclassical treatment: the WKB approximation for the propagation of the wave functions *between* the avoided crossings and the computation of the transition amplitudes *in the crossings* by Landau-Zener-Stückelberg matrices.

Between the avoided crossings we assume the stationary wave functions to follow adiabatically the potential curves. The two general solutions of the single-channel Schrödinger equation (3.9) for waves propagating in the $(\pm y)$ directions read

$$\alpha^{\pm}_{n_i}(y) = \frac{1}{\sqrt{p_{n_i}(y)}} \exp\left\{\pm\frac{i}{\hbar}\int^{y} p_{n_i}(y')\,dy'\right\}, \qquad (3.11)$$

where $p_{n_i}(y) = \sqrt{2m[T_{\infty y} - W_{n_i}(y)]}$ is the quasiclassical momentum.

On the other hand, in the region close to narrow avoided crossings the change of the eigenvectors of $\hat{H}_1$ with respect to y is very important for the evolution of the wave function. In our approximate treatment we allow for nonadiabatic behavior in the allowed potentials *only* near the avoided crossings. As is well known from the theory of atomic collisions, such transitions at each single crossing can be described in a two-state approximation and the Landau-Zener-Stückelberg treatment leads to (2×2) unitary transition matrices [17] for constant atomic velocity. For the wave mechanical construction of the diffraction amplitudes we have adapted an ansatz from collision theory [18] to obtain the forward propagation of the wave functions α_{n_i} and $\alpha_{n_{i+1}}$, $i = 1, 2, \ldots$ across an avoided crossing between the potentials W_{n_i} and $W_{n_{i+1}}$, including the varying momentum [see Fig. 5(b)]. The ansatz neglects reflection due to the crossing and therefore assumes a level spacing which is much less than the kinetic energy in the crossing [19]. The explicit expression of the transition matrices is given in Appendix B 1.

3. *Low-velocity regime*

The atomic dynamics in the potentials W_{n_I} and $W_{n_{II}}$, in particular near classical turning points, is complicated by the fact that the slow atoms may be nonadiabatically coupled to the asymptotically forbidden potential W_{n_I}.

The physical processes that govern transmission and reflection of the wave $\alpha_{n_{II}}$ in the adiabatic potential $W_{n_{II}}$ are [see Fig. 5(a)] (i) barrier reflection, if the top of the $W_{n_{II}}$ barrier is classically forbidden; (ii) adiabatic motion and overbarrier reflection in $W_{n_{II}}$, if $T_{\infty y}$ slightly exceeds the maxima of the potential $W_{n_{II}}$; (iii) coupling to quasibound states in the wells of W_{n_I} resulting in reflection resonances for the outgoing amplitudes $\alpha_{n_{II}}$, if the wells of W_{n_I} are classically allowed. They are discussed in more detail in Sec. IV.

To proceed to the total description of the diffraction process the incoming de Broglie wave has to be mapped onto the diffracted waves. This mapping has to take into account the splitting of the incoming wave into several partial waves at avoided crossings. The simultaneous motion of all the partial waves has to be traced through the potentials of the high- and low-velocity regime. Different reflected partial waves interfere in the outgoing diffraction orders.

In Appendix B we outline a systematic calculation of this superposition in the adiabatic basis. The mapping of the incoming onto the outgoing waves will be composed from semiclassical propagators for adiabatic motion and nonadiabatic transitions in the *high-velocity regime*, as well as from reflection and transmission amplitudes extracted from a full quantum-mechanical treatment of the *low-velocity regime*.

IV. DISCUSSION OF THE PREDICTED DIFFRACTION PATTERNS

In this section we discuss diffraction patterns resulting from the physical picture of Secs. III A–III C which have been calculated numerically as described in Appendix B.

The performance of the reflection grating depends mainly on the following parameters: the laser detuning Δ, the Doppler detuning Δ_D [Eq. (2.12)], the Rabi frequencies Ω_+ and Ω_- of the copropagating and counterpropagating light waves, and the atomic beam properties.

A. Dependence on the angle of grazing incidence

In this section we present the numerically calculated population of diffraction orders as a function of the angle of grazing incidence α. In the regime of grazing incidence the main effect of varying α is to vary the perpendicular momentum $p_{\infty y} = |\mathbf{p}_\infty| \sin\alpha$ since the parallel momentum $p_{\infty x} = |\mathbf{p}_\infty| \cos\alpha$ almost coincides with the total momentum $|\mathbf{p}_\infty|$.

The calculation is performed for two examples: first for a thermal atomic beam and second for a decelerated atomic beam. The total atomic velocity $\frac{|\mathbf{p}_\infty|}{m}$ has a striking effect on the diffraction pattern as will be discussed in the following. The light-induced shift of the diabatic curves has to exceed the asymptotic energy separation of the quasipotentials to induce avoided crossings necessary for diffraction. This energy separation scales linearly with the longitudinal Doppler shift $\Delta_D = Q\frac{p_{\infty x}}{m}$ [see Eq. (3.6) and Fig. 4(a)]. Thus the minimum laser intensity to produce a sufficient light shift depends linearly on the value of $p_{\infty x}$ (and therefore on $|\mathbf{p}_\infty|$).

As a first example we consider a thermal atomic beam (600 m/s) under grazing incidence ($\alpha \lesssim 6$ mrad) and a laser intensity of the order of a few 100 mW/mm^2. This combination of parameters does not yet meet the condition mentioned above. Nonadiabatic population transfer to diffracted orders will be negligible, thus only barrier reflection in the zeroth order is expected (see Fig. 6).

In contrast to this, the regime of avoided crossings (i.e., of considerable mixing of the diffraction orders) is reached either by increasing the laser intensity or by decreasing the total atomic velocity, e.g., by laser slowing. Deceleration has the additional advantage of an increased atomic de Broglie wavelength and, as a consequence, an enhanced angular separation of the diffracted beams. Diffraction patterns are calculated as a function of the angle of grazing incidence α, for very slow atoms (20 m/s) allowing much larger angles $\alpha \lesssim 100$ mrad [other parameters given in Fig. 4(a)]. The populations of the diffraction orders vary very rapidly with α and exhibit a great variety of structure (Fig. 7). This will be explained in the following (refer to Figs. 7 and 8).

For small angles, α=0–40 mrad, the kinetic energy $T_{\infty y}$ proportional to $(\sin\alpha)^2$ is small compared to the first potential barrier of $W_{n_{II}}$ ($n_{II} = 0$) [Fig. 8(a)] and the atoms are completely reflected in the zeroth order [Fig. 7(a)]. At an angle of $\alpha = 46$ mrad the energy $T_{\infty y}$ slightly exceeds all barriers of $W_{n_{II}}$. Thus the motion in the low-velocity regime is entirely adiabatic and, because the potential varies slowly on the scale of the de Broglie wavelength, reflection is negligible [Fig. 7(a)].

In the intermediate range, α=47–58 mrad, nonadiabatic coupling to quasibound states in the wells of the partially forbidden potential W_{n_I} begins to play an important role [Fig. 8(b)]. They give rise to two series of re-

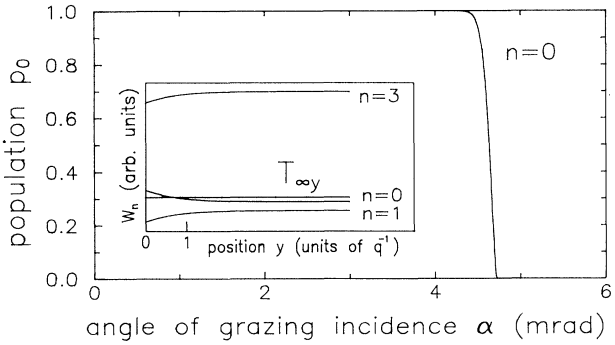

FIG. 6. Populations of diffraction orders for a thermal atomic beam. Specular reflection of the zeroth diffraction order showing up for a thermal atomic beam (total atomic velocity 600 m/s): Optimized parameters are $\Omega_+(0) = \Omega_-(0) = 10 \times 10^4\Delta_q$, $\Delta = 23 \times 10^4\Delta_q$, $\Delta_D = 20 \times 10^4\Delta_q$. The inset shows the relevant quasipotentials.

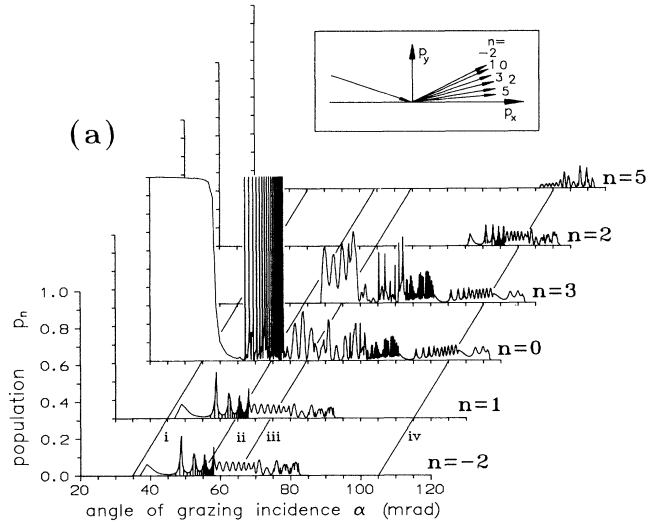

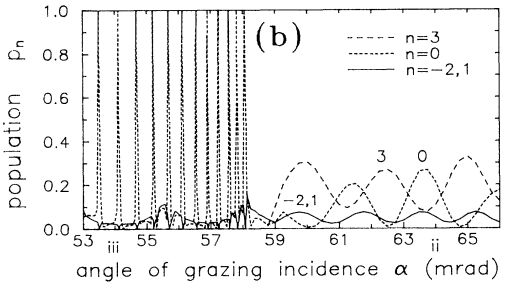

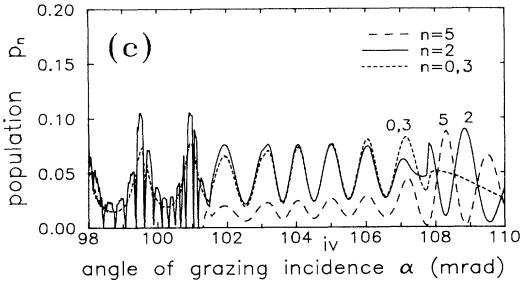

FIG. 7. Populations of diffraction orders for a slow atomic beam: (a) Overview: data have been calculated for parameters as in Fig. 4 (a) and varying angle of grazing incidence α corresponding to varying $T_{\infty y}$. The inset shows the ordering of the outgoing beams with respect to their angle with the surface. Note that they are sorted by the magnitude of $p_{\infty y,n}$ but not by the order n. The reason for this is that only the odd orders depend on the detuning [see Eqs. (3.2) and (3.6)]. Quasipotentials for the angles marked by (i)–(iv) are shown in Fig. 8. (b) Detailed view from (a): populations of diffraction orders $n = -2, 1, 0, 3$ in the range α=53–66 mrad. (c) Detailed view from (a): populations of diffraction orders $n = 0, 3, 2, 5$ in the range α=98–110 mrad.

flection resonances: in the diffraction populations $n = 0$ and in $n = -2, 1$; a densely spaced one, displayed in Fig. 7(b) from $\alpha = 53$ mrad to 58 mrad; and a widely spaced one, displayed in Fig. 7(b) from $\alpha = 53$ mrad to 66 mrad. The spacing between the resonances depends on the shape of the wells and approximately obeys a Bohr Sommerfeld quantization condition. The widths of the resonances depend on the losses due to nonadiabatic transitions out of the wells and vary slowly with $T_{\infty y}$. Atoms that are not reflected into $n = 0$ by reflection resonances of the first well of W_{n_I} may pass the first crossing between $W_{n_{II}}$ and W_{n_I} adiabatically and couple to a second set of quasibound states located at the second well of W_{n_I}. The reflection resonances of this second, narrower potential well show both wider width and spacing.

For increasing angle of incidence, $\alpha > 58,7$ mrad, the channel $n = 3$ becomes allowed [Figs. 7(b) and 8(c)]. As a consequence quasibound states and resonances of $n = 0$ disappear. Instead of this, the incoming wave simply splits in the first crossing. One fraction is reflected at the first classical turning point of W_{n_I} while the other fraction couples to quasibound states in the second well of W_{n_I}. In the first crossing the waves reflected by the first and second turning point interfere [Fig. 8(c)] giving rise to Stückelberg oscillations as a function of $T_{\infty y}$ in the channels $n_{II} = 0$ and $n_I = 3$. These resonances are modulated by the resonance structure of the second well [Figs. 7(a) and 7(b)].

Finally, for angles $\alpha > 85$ mrad the set of reflected diffraction orders has changed [Fig. 8(d)]: Since the angles of the outgoing orders $n = -2, 1$ exceed the maximum permitted angle [see Eq. (3.10)] the population of these diffraction orders vanishes. At the same time the orders $n = 2, 5$, lying at small angles with the surface, become energetically allowed. The second potential well of W_{n_I} ($n_I = 5$) is connected with $n = 0$ in the asymp-

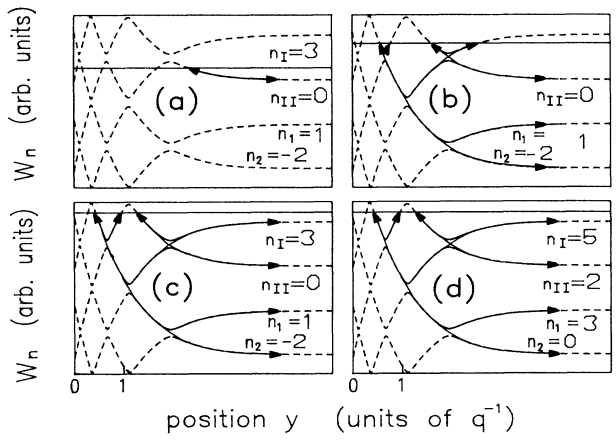

FIG. 8. Quasipotentials corresponding to Fig. 7. Magnified parts of Fig. 4(a), showing relevant quasipotentials. Horizontal lines denote the value of the energy $T_{\infty y}$. (a)–(d) refer to the angles of grazing incidence marked by (i)–(iv) in Fig. 7: (a) $\alpha = 35$ mrad, (b) $\alpha = 56$ mrad, (c) $\alpha = 64$ mrad, (d) $\alpha = 105$ mrad.

totic region by a diabatic curve. Therefore a de Broglie wave incoming in $n = 0$ has to behave nonadiabatically at each encountered crossing to populate this second potential well. On the other hand, the first well of W_{n_I} cannot be reached directly by the incoming wave. It may exclusively be populated by outgoing waves starting from the second well. Therefore the resonance structure due to quasibound states of the first well of W_{n_I} now shows up in reflecting the outgoing wave in $n = 0$ back to the surface. This causes closely spaced zeros in the population of the order $n = 2$ in the neighborhood of $\alpha = 100$ mrad [Figs. 7(a) and 7(c)].

B. Averaging over beam divergence

The rapid variation of the populations with the energy $T_{\infty y}$ is due to the variation of the semiclassical WKB phases of the waves. These phases depend strongly on all parameters which determine the shape of the potentials and on the asymptotic kinetic energy $T_{\infty y}$. In a real experiment the narrow resonance structures may not be resolved because of imperfections, e.g., of the atomic beam preparation or of the intensity profile of an evanescent wave produced by a real laser mode. We take into account a small angular divergence corresponding to an atomic beam in the transversal recoil limit, thus having a beam divergence of 2 mrad. The data from Fig. 7 have to be convoluted with a Gaussian velocity distribution with the width of 2 mrad. The resulting curves vary more slowly with the angle of incidence. Averaging over other parameters of the problem will yield similar, slow variations of the reflection and transition probabilities (see Fig. 9).

C. Variation of the running wave proportion (Ω_+/Ω_-): From diffraction to reflection

Changing from the standing-wave case $(\Omega_+ = \Omega_-)$ to the running-wave case $(\Omega_+ \gg \Omega_-)$ smoothly turns the system from a diffraction into a reflection device. How does this transition appear in the adiabatic model? For a pure standing wave $(\Omega_+ = \Omega_-)$ and the particular parameters given in Fig. 4(a) only weak nonadiabatic transitions occur between adiabatic states. Nearly all of the incoming wave reaches the surface in the $n = 0$ adiabatic potential. Consequently the reflectivity is negligible.

If we now consider a continuous transition from $\Omega_+ = \Omega_-$ to $\Omega_+ \gg \Omega_-$, we remark that the energy splittings of all avoided crossings approach zero. In the limit $\Omega_- = 0$ the effective Hamiltonian $H_1(y)$ (3.6) decouples completely into a set of uncoupled two-level Hamiltonians. Thus their quasipotentials *do cross*, because they belong to uncoupled states. In this case, the overall behavior in the quasipotential pattern becomes purely diabatic. The incoming wave is completely reflected by a repulsive diabatic curve, while the efficiency of populating different diffraction orders drops to zero.

Optimum distribution of the incoming population among various diffraction orders occurs in an *intermediate* regime between the diabatic regime and the adiabatic regime. Thus *maximum reflectivity* and *optimum population of higher orders* cannot be obtained for the same experimental parameters. Figure 10 confirms this qualitative discussion and shows that the value of $(\Omega_+/\Omega_-) = 2.33$ chosen for the example discussed above is optimum for even diffraction orders, at the expense of total reflectivity (see Sec. IV E).

For the parameters chosen in Fig. 10 it is not important whether the copropagating or the counterpropagation laser wave is dominant. Dominant copropagating wave Ω_+ couples $n = 0$ to 1 whereas dominant counterpropagating wave Ω_- couples $n = 0$ to -1. However, in both cases the limiting situation is a two-level reflection system with positive effective detuning (approximately given by $\Delta - \Delta_D$).

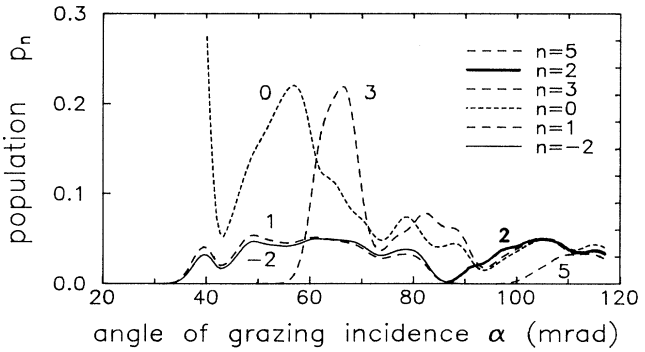

FIG. 9. Populations of diffraction orders, calculated assuming imperfect collimation of the incident atomic beam: Data from Fig. 7 are convoluted with a Gaussian distribution of the angle of grazing incidence α with the Gaussian width $\sigma(\alpha) = 2$ mrad.

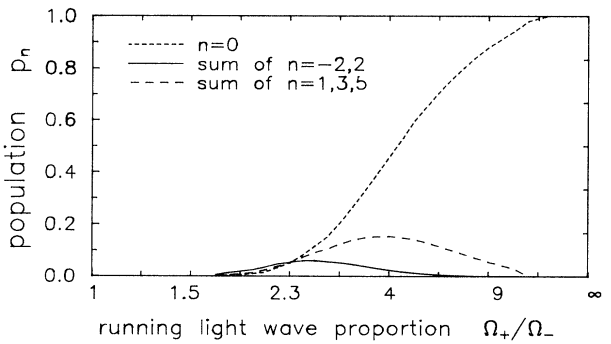

FIG. 10. Populations of diffraction orders for varying running wave proportion (Ω_+/Ω_-): angle of grazing incidence $\alpha = 105$ mrad (corresponding to $T_{\infty y} = 2.1 \times 10^4 \hbar\Delta_q$), other parameters are the same as in Fig. 4(a). The ratio (Ω_+/Ω_-) varies while the sum $(\Omega_+ + \Omega_-) = 1 \times 10^6 \Delta_q$ is kept constant. Intensities of the diffraction orders are averaged over a symmetric interval around $T_{\infty y}$ [corresponding to a angular uncertainty $\sigma(\alpha) = 2$ mrad] as in Fig. 9, thus removing rapid oscillation. The optimum for the even diffraction orders shows up for $\Omega_+/\Omega_- = 2.33$. This is the running wave proportion chosen in Figs. 4(a) and 7–9.

D. Variation of the laser detuning

Varying the detuning Δ has two effects: First, it shifts the odd levels in the asymptotic region and changes the sequence of the odd versus the even diffraction orders. Second, with increasing detuning Δ the energy separation in avoided crossings approaches zero. Thus one reaches the diabatic regime and specular reflection predominates, similar to the behavior discussed in the preceding paragraph. As a second effect of increasing detuning the slope as well as the maximum value of the light shift decreases. In the limit $\Delta \to \infty$ the diabatic curve is not sufficiently shifted by the interaction to exceed the energy $E = T_{\infty y}$, and is no longer repulsive. In our example (Fig. 11) the diabatic regime is reached before the reflecting barrier decreases too much.

Figure 11 shows that the value of the detuning $\Delta = 1.3 \times 10^4 \Delta_q$ chosen for the example given above is optimized for even diffraction orders. As both the running wave proportion (Ω_+/Ω_-) and the detuning Δ affect the nonadiabatic transition probabilities in nearly the same way, there is a strong interdependence of (Ω_+/Ω_-) and Δ.

E. Optimizing even diffraction orders

The suitability of the atomic diffraction grating as a beam splitter for atomic interferometry depends on the possibility of populating even diffraction orders significantly. Remember that even orders refer to ground-state atoms in the asymptotic region, whereas excited-state atoms may decay after leaving the grating. Therefore we optimize the populations of *even* orders by finding a suitable combination of the running-wave proportion (Ω_+/Ω_-) and the detuning Δ (see Figs. 10 and 11).

In our example (Ω_+/Ω_-) and Δ are chosen in order to make transition probabilities of the relevant avoided crossings approximately equal to the value 1/2. This is appropriate because the avoided crossings themselves can be visualized as de Broglie wave beam splitters. This circumstance causes the principle limitation in optimizing the populations of the even diffraction orders $n = \pm 2$: As one can see from Fig. 4(a), the transfer of population from the incident order $n = 0$ to ± 2 requires at least four avoided crossings. While one of these avoided crossings has to be passed *diabatically* by the incoming wave, it has to be followed *adiabatically* by an outgoing wave. Thus the best compromise is a transition probability for this crossing of 1/2. Since the transition probabilities are very similar at all crossings, also the neighboring crossings will have transition probabilities close to 1/2. A wave that passes four avoided crossings will then have at maximum the population $\left(\frac{1}{2}\right)^4 = \frac{1}{16}$, provided there is complete reflection due to a resonance of a quasibound state. Averaging over α adds a factor of approximate $\frac{1}{2}$. Thus the averaged population of even diffraction orders cannot be expected to be much larger than 3%. However, optimized populations of about 6% (see Fig. 9) can be achieved by carefully balancing the slightly different effect of the detuning and the running-wave proportion on the nonadiabatic transitions. Note that the optimum for diffraction into even orders is different from the optimum for diffraction into odd orders (mainly n=3) and far off the conditions giving a total reflectivity of 100% (mainly n=0) (Figs. 10 and 11).

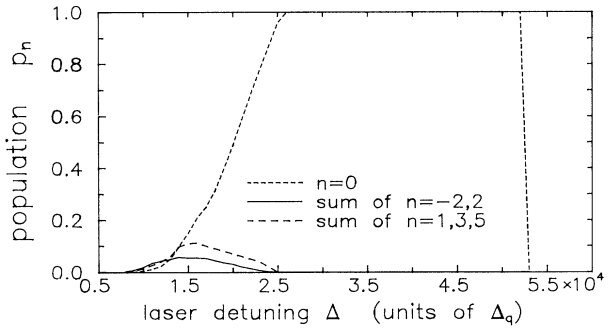

FIG. 11. Populations of diffraction orders for varying laser detuning: angle of grazing incidence $\alpha = 105$ mrad (corresponding to $T_{\infty y} = 2.1 \times 10^4 \hbar \Delta_q$), other parameters are the same as in Fig. 4(a). The laser detuning varies. Populations of the diffraction orders are averaged over an interval around $T_{\infty y}$ [corresponding to a angular uncertainty $\sigma(\alpha) = 2$ mrad] as in Fig. 9 thus removing rapid oscillation. The optimum for the even diffraction orders shows up for $\Delta = 1.3 \times 10^4 \Delta_q$. This is the laser detuning chosen in Figs. 4 and 7–9.

V. CONCLUSION

We have studied the light-induced atomic reflection grating using an adiabatic approximation for the motion perpendicular to the grating. The transition from the incoming de Broglie wave to the diffracted waves is viewed as an inelastic redistribution of energy from internal motion and parallel motion into the perpendicular motion. This redistribution takes place via splitting and recombination of dressed-state de Broglie waves at avoided crossing of quasipotentials.

Our model of the diffraction process allows a numerical construction of the diffraction pattern yielding important conclusions about the operation of atomic beam splitters. Most strikingly, because of the interplay of adiabatic motion and nonadiabatic transitions, the function of atomic beam reflection and redistribution of population among higher diffraction orders cannot be optimized simultaneously. It turns out, however, that a significant running-wave contribution to the standing wave improves the performance of the reflection grating considerably. As the light shift has to exceed the longitudinal Doppler shift to produce an avoided level crossing, slow atoms are required to achieve optimum diffraction. Characteristic features of the avoided crossings can be tuned by varying experimental parameters like laser detuning and running-wave Rabi frequencies. These features directly influence the diffraction patterns.

The outgoing diffraction orders, distinguished by their different center-of-mass motion, are correlated with different internal states. Because of the wide angular separation of the outgoing waves, the evanescent wave mirror

or grating provides interesting applications for quantum measurement problems [20].

Our theoretical method is similarly well suited to perform a nonperturbative analysis of the well-known Kapitza-Dirac diffraction of an atomic beam traversing a perpendicular standing light field. As it is a wave mechanical model the coupling to the vacuum field, which would, however, reduce the diffraction and reflection performance, is not allowed for. Using recently proposed algorithms to simulate spontaneous emission with wave functions [21], an extension of our description seems possible.

Our ansatz, using quasipotentials, is suitable to be extended by taking into account additional potentials of surface interactions. Monitoring the reflection probability of the atoms while varying the height of the light force barrier might yield valuable information on the surface potentials.

ACKNOWLEDGMENT

We acknowledge financial support by the Deutsche Forschungsgemeinschaft.

APPENDIX A: NONADIABATIC TRANSITIONS FOR THE ATOMIC REFLECTION

In this appendix we compute the wave function $(\eta_1(y),\eta_2(y))^t$ of the Hamilton operator $\hat{H}=\hat{H}_A+\hat{H}_{\rm NA}$ (2.29) for the reflection problem (Sec. II C), now containing the derivatives of the eigenvectors (2.20). Evaluation of $\hat{H}_{\rm NA}$ (2.30) shows that for strong reflection $\hat{H}_{\rm NA}$ provides only a small perturbation. Thus the perturbed wave function $(\eta_1(y),\eta_2(y))^t$ is nearly identical to the unperturbed eigenfunction of the adiabatic Hamiltonian H_A. This unperturbed wave function is obtained as the solution of (2.23) for a reflected ground-state wave in the repulsive potential W_2, thus reading $(0,\alpha_2(y))^t$. The solution (η_1,η_2) can be computed from this, using a distorted-wave approximation.

We start from the integral equation which is equivalent to the *perturbed* Schrödinger equation $T_{\infty y}(\eta_1(y),\eta_2(y))^t=(\hat{H}_A+\hat{H}_{\rm NA})(\eta_1(y),\eta_2(y))^t$. It is obtained using Wronski's theorem and two linear independent *unperturbed* solutions $(\alpha_1^+,\alpha_2^+)^t$ and $(\alpha_1^-,\alpha_2^-)^t$ [22]

$$\eta_1(y)=0+\frac{1}{2i}\int_{-\infty}^{+\infty}\alpha_1^-(y_<)\alpha_1^+(y_>)\times\{(\hat{H}_{\rm NA})_{11}\eta_1+(\hat{H}_{\rm NA})_{12}\eta_2\}\Big|_{y'}dy', \tag{A1}$$

$$\eta_2(y)=\alpha_2(y)+\frac{1}{2i}\int_{-\infty}^{+\infty}\alpha_2^-(y_<)\alpha_2^+(y_>)\times\{[\hat{H}_{\rm NA})_{21}\eta_1+(\hat{H}_{\rm NA})_{22}\eta_2\}\Big|_{y'}dy', \tag{A2}$$

where $y_<=\min(y,y')$ and $y_>=\max(y,y')$. The products $\alpha_n^-(y_<)\alpha_n^+(y_>)$ $(n=1,2)$ are Green's functions. They are defined by the asymptotic behavior of the two unperturbed solutions $\alpha_n^\pm$ $(n=1,2)$

$$\alpha_n^\pm(y)\underset{y\to-\infty}{\longrightarrow}\frac{1}{\sqrt{p_n}}\exp\left\{\pm\frac{i}{\hbar}p_n y\right\}, \tag{A3}$$

where $p_n=\sqrt{2m[T_{\infty y}-W_n(y)]}$. Thus in the WKB region the Green's functions of the integral equation reduce to $(n=1,2)$

$$\alpha_n^-(y)\alpha_n^+(y')=\frac{1}{\sqrt{p_n(y)p_n(y')}}\exp\left\{\frac{i}{\hbar}\left|\int_y^{y'}p_n(\tilde{y})\,d\tilde{y}\right|\right\}. \tag{A4}$$

The integral equation (A2) includes the boundary condition of a pure incoming ground-state wave $(0,\alpha_2^-(y))^t$ and additional outgoing waves. Because of $(\eta_1(y),\eta_2(y))^t$ being nearly equal to the unperturbed solution $(0,\alpha_2(y))^t$, the distorted-wave approximation is performed by substituting $(\eta_1(y),\eta_2(y))^t$ by $(0,\alpha_2(y))^t$ on the right-hand side of (A2). To this degree of the approximation the wave function in the repulsive potential W_2 remains unperturbed while the effect of $\hat{H}_{\rm NA}$ is to create a nonvanishing wave function in the attractive potential W_1. Because of W_1 meeting the condition for applying the WKB approximation [Eq. (A4)] can be used to give an explicit expression for η_1. As we are interested merely in the transition probability we supress the diagonal element $(\hat{H}_{\rm NA})_{11}$. Thus

$$\eta_1(y)=\frac{-i}{2\sqrt{p_2(y)}}\int_{-\infty}^{+\infty}\frac{1}{\sqrt{p_2(y')}}\exp\left\{\frac{i}{\hbar}\left|\int_y^{y'}p_2(\tilde{y})\,d\tilde{y}\right|\right\}\{(\hat{H}_{\rm NA})_{12}(y')\alpha_2(y')\}\,dy' \tag{A5}$$

is the wave function in W_1. In $y=0$ the wave function α_2 vanishes because of tunneling into the barrier W_2 whereas for $y\to\infty$ the perturbation matrix element $\hat{H}_{\rm NA}$ vanishes as the angle Θ of the eigenvector basis approaches the constant value zero. According to the boundary conditions of outgoing waves incorporated in the Green's function, η_1 is an entirely incoming wave at $y=0$ and an entirely outgoing wave for $y\to\infty$. The total outgoing current of η_1 can be evaluated as the sum of the currents at $y=0$ and for $y\to\infty$. Thus the total nonadiabatic loss $L_{\rm NA}$ is given by the probability per reflection

$$L_{\rm NA}=(|p_1(0)||\eta_1(0)|^2+\lim_{y\to\infty}|p_1(y)||\eta_1(y)|^2)\,. \tag{A6}$$

The numerical evaluation of (A5) and (A6) is greatly

simplified by the analytic expressions for the wave function α_2 as well as for the exponential factors $\int p\,dy$. WKB expressions are used for the wave function α_2 everywhere except a small region around the classical turning point, where Airy functions are used. By the substitution $z = \exp(-y)$ the exponential factors $\int p\,dy$ get the form

$$\int p_{1,2}\,dy = \sqrt{\frac{\Omega(0)}{2}} \int \sqrt{g \pm \sqrt{d^2+z^2}}\ \frac{dz}{z},$$

where $g \equiv \frac{2T_{\infty y}+\Delta_{\rm eff}}{\Omega(0)}$ and $d \equiv \frac{\Delta_{\rm eff}}{\Omega(0)}$. The upper sign refers to the index 1 the lower to 2. Another substitution $r = \sqrt{d^2+z^2}$ leads to a standard integral formula [23] which yields

$$\int_{y_1}^{y_2} p_{1,2}\,dy = -\sqrt{\frac{\Omega(0)}{2}}\left[4\sqrt{g\pm r} + \sqrt{g\mp d}\,\ln\left(\frac{(\sqrt{g\pm r}-\sqrt{g\mp d})}{(\sqrt{g\pm r}+\sqrt{g\mp d})}\right) + \sqrt{g\pm d}\,\ln\left(\frac{(\sqrt{g\pm r}-\sqrt{g\pm d})}{(\sqrt{g\pm r}+\sqrt{g\pm d})}\right)\right]_{r(y_1)}^{r(y_2)}. \tag{A7}$$

The integrand of (A5) turns out to be a rapid oscillating function. For decreasing values of the nonadiabatic loss $L_{\rm NA} \lesssim 10^{-10}$ the numerical evaluation of (A6) is increasingly affected by contributions of roundoff noise, truncation errors and dominantly by errors resulting from the piecewise definition of the wave function. However, the result for $L_{\rm NA}$ given in Fig. 3 represents a suitable upper bound for the nonadiabatic loss.

APPENDIX B: COMPUTATION OF THE OUTGOING DIFFRACTED WAVES

In this appendix the total wave function is constructed to obtain the populations of the outgoing diffraction orders. The physical predictions obtained from this construction, which is presented in more detail in the following, are discussed in Sec. IV.

The propagation of the atomic de Broglie wave is assumed to be piecewise adiabatic, perturbed by nonadiabatic transitions at the avoided crossings. Sections B 1 and B 2 are devoted to deriving the propagators Eqs. (B3), (B4), and (B7) for both adiabatic and nonadiabatic motion. We then want to unite all these elements to construct transmission and reflection matrices $T^{\pm}$, $R^{\pm}$ as well as transition matrices $S^{\pm}$ for the simultaneous propagation of the wave function in the potentials W_n. We divide the y axis from the asymptotic region to the surface into intervals defined by suitably chosen points $y_1,\ldots,y_m,\ldots,y_M$ [see Fig. 4(a)]. The point y_M is chosen in the asymptotic region, whereas the points $y_1,\ldots,y_{M-1}$ are the locations of those special avoided crossings that connect the high-velocity regime with the low-velocity regime. Our method requires the knowledge of the total wave function

$$\mathcal{A}^{\pm}(y) \equiv (\alpha^{\pm}_{n_{\rm I}}(y), \alpha^{\pm}_{n_{\rm II}}(y), \alpha^{\pm}_{n_1}(y), \alpha^{\pm}_{n_2}(y), \ldots)^t \tag{B1}$$

only at one end point per interval. The total mapping of the incoming de Broglie wave to the outgoing waves is given in Appendix B 3.

1. Semiclassical propagators for the high-velocity regime

Following Eqs. (3.9) and (3.11) the relative amplitude $c_{i,i+1}(y,y')$ for the propagation of a wave in W_{n_i} from y' to y is given by

$$\alpha^{\pm}_{n_i}(y) = c_i(y,y')\,\alpha^{\pm}_{n_i}(y'), \tag{B2}$$

where the upper index + refers to propagation in the $+y$ direction and $y \geq y'$. Semiclassically this propagator reads

$$c_i(y,y') = \sqrt{\frac{p_{n_i}(y')}{p_{n_i}(y)}}\ \exp\left\{\frac{i}{\hbar}\int_{y'}^{y} p_{n_i}(\tilde{y})\,d\tilde{y}\right\}. \tag{B3}$$

The $c_i(y,y')$ obey the relation $c_i(y,y')c_i(y',y) = 1$. The above propagators apply for intervals between avoided crossings.

At avoided crossings we allow for nonadiabatic transitions. For the two possible directions of propagation we introduce unitary matrices for the nonadiabatic transitions at an avoided crossing in $y_{\rm AC}$ (here $y_{\rm AC}$ denotes the position of the minimum energy separation between two potential curves)

$$\begin{pmatrix} \alpha^{\pm}_{n_i}(y_{\rm AC}\pm\epsilon) \\ \alpha^{\pm}_{n_{i+1}}(y_{\rm AC}\pm\epsilon) \end{pmatrix} = s^{\pm}_{i,i+1}(y_{\rm AC}) \begin{pmatrix} \alpha^{\pm}_{n_i}(y_{\rm AC}\mp\epsilon) \\ \alpha^{\pm}_{n_{i+1}}(y_{\rm AC}\mp\epsilon) \end{pmatrix}. \tag{B4}$$

The upper signs refer to waves propagating in the $+y$ direction, the lower signs to waves going in the $-y$ direction. Here and in the following $y \pm \epsilon$ is used as an abbreviation for the one-sided limit $\lim_{\epsilon\to 0}(y \pm \epsilon)$ with $\epsilon > 0$. The transition matrix $s^{\pm}_{i,i+1}$ is given by

$$s^{\pm}_{i,i+1}(y_{\rm AC}) = \begin{pmatrix} \sqrt{1-\rho^2} & \mp\rho e^{\mp i\chi} \\ \pm\rho e^{\pm i\chi} & \sqrt{1-\rho^2} \end{pmatrix}, \tag{B5}$$

where $\rho = e^{-{\rm Im}(\varphi)}$ and $\chi = {\rm Re}(\varphi)$. In Ref. [18] it is shown that the complex quantity φ can be obtained by path integration in the complex plane,

$$\varphi = \frac{1}{\hbar}\int_{y_{\rm AC}}^{Y_*} [p_{n_{i+1}}(y) - p_{n_i}(y)]\,dy\,, \tag{B6}$$

where the path leads from the avoided crossing on the real axis $y_{\rm AC}$ to the intersection point Y_* of the potentials W_{n_i} and $W_{n_{i+1}}$ [24]. Since the transition amplitudes are given by the classical action integrated to and from the complex transition point, the relation $s^{-}_{i,i+1}(y_{\rm AC}) = [s^{+}_{i,i+1}(y_{\rm AC})]^{\dagger}$ holds. We have verified numerically that the two-state approximation is actually justified for all relevant narrow

crossings, i.e., those that cause transition probabilities larger than a few percent.

2. Quantum-mechanical reflection and transmission amplitudes for the low-velocity regime

The above techniques cannot be applied for atoms moving slowly in the two highest potentials because the de Broglie wavelength will no longer be small compared to the range of the avoided crossing and nonadiabatic coupling will be important throughout the interval and notably at the avoided crossing. For this situation we therefore proceed to a numerical calculation of the transmission and reflection coefficients.

Generally the wave amplitudes in y_m depend linearly on the amplitudes in y_{m-1} and y_{m+1}. The wave amplitudes $\alpha^{\pm}_{n_\mathrm{I}}$ in the uppermost potential are negligible in the points y_m, because these points are energetically forbidden for atoms in the state n_I. Thus we introduce for each open interval (y_m, y_{m+1}) [see Fig. 5(a)] transmission and reflection amplitudes $t^{\pm}(y_m, y_{m+1})$ and $r^{\pm}(y_m, y_{m+1})$ relating only amplitudes in the potential n_II with each other, for both propagation directions along the y axis [25] [for clearness the argument (y_m, y_{m+1}) of the $t^{\pm}$ and $r^{\pm}$ is suppressed]

$$\begin{pmatrix} \alpha^{-}_{n_\mathrm{II}}(y_m) \\ \alpha^{+}_{n_\mathrm{II}}(y_{m+1}) \end{pmatrix} = \begin{pmatrix} r^{+} & t^{-} \\ t^{+} & r^{-} \end{pmatrix} \begin{pmatrix} \alpha^{+}_{n_\mathrm{II}}(y_m) \\ \alpha^{-}_{n_\mathrm{II}}(y_{m+1}) \end{pmatrix} . \tag{B7}$$

Though Eq. (B7) seems to involve the motion in the potential W_{n_II} only, actually the reflection and transmission amplitudes are strongly affected by the nonadiabatic coupling to the asymptotically forbidden potential W_{n_I} particularly if resonances of quasibound states in W_{n_I} are excited. To obtain these amplitudes we perform a numerical integration of the Schrödinger equation for both α_{n_I} and α_{n_II}, conveniently carried out in a local diabatic representation

$$\frac{d^2}{dy^2} \begin{pmatrix} \alpha_{n_\mathrm{I}}(y) \\ \alpha_{n_\mathrm{II}}(y) \end{pmatrix} = \begin{pmatrix} -T_{\infty y} + D_a(y) & C(y) \\ C(y) & -T_{\infty y} + D_b(y) \end{pmatrix} \begin{pmatrix} \alpha_{n_\mathrm{I}}(y) \\ \alpha_{n_\mathrm{II}}(y) \end{pmatrix} . \tag{B8}$$

Here $D_{a,b}$ denote diabatic potential curves and C a corresponding coupling; their form has been fitted from the adiabatic quasipotentials $W_{n_{\mathrm{I,II}}}$. As the amplitudes α_{n_I} and α_{n_II} have to be expanded in forward and backward propagating waves, Eq. (B8) yields a four-dimensional first-order differential equation. The boundary conditions have to take into account the behavior of α_{n_I} and α_{n_II} at the end points of the open interval (y_m, y_{m+1}): while the amplitudes α_{n_II} consist of traveling waves, the amplitudes α_{n_I} are exponentially decaying in energetically forbidden regions. From the result of the integration we read off reflection and transmission amplitudes for Eq. (B7).

Slightly more complicated is the situation in the interval (y_{M-1}, y_M) close to the asymptotic region: here the potential W_{n_I} may be asympotically accessible. As a consequence, instead of four elements as in Eq. (B7), nine elements have to be determined, connecting $\alpha^{\pm}_{n_\mathrm{I}}(y_M)$ and $\alpha^{\pm}_{n_\mathrm{II}}(y_M)$ with $\alpha^{\pm}_{n_\mathrm{II}}(y_{M-1})$. These nine amplitudes are again computed numerically from Eq. (B8). If on the other hand W_{n_II} as well as W_{n_I} are asymptotically inaccessible, there is only one nonvanishing coefficient $r_{+}(y_{M-1}, y_M)$ which can be obtained by a WKB treatment for barrier reflection of $\alpha^{+}_{n_\mathrm{II}}(y_{M-1})$.

3. Interference of reflected de Broglie waves

From the semiclassical scalar propagators $c_i(y, y')$ [Eq. (B3)], the (2×2) transition matrices $s^{\pm}_{i,i+1}$ [Eq. (B4)], and the transmission and reflection amplitudes $t^{\pm}, r^{\pm}$ [Eq. (B7)] we will construct matrices $T^{\pm}, R^{\pm}, S^{\pm}$ that allow us to trace the simultaneous propagation of the atomic de Broglie wave $\mathcal{A}^{\pm}$ [Eq. (B1)] through the multichannel potential. Each classical turning point, at best one per interval (y_m, y_{m+1}), generates a reflected de Broglie wave which interferes with all other reflected contributions. This interference bears some similarity to the propagation of a light ray through a mirror formed by a pile of dielectric layers. In our calculation we keep track of all the amplitudes and propagate them back to the asymptotic region passing several avoided crossings and thus populating other diffraction orders.

The total diffraction pattern is computed as follows. First consider an open interval (y_m, y_{m+1}) and two incoming vectors $\mathcal{A}^{+}(y_m + \epsilon)$ and $\mathcal{A}^{-}(y_{m+1} - \epsilon)$ [see Eq. (B1)] defined at the respective interval boundaries. The resulting outgoing vectors $\mathcal{A}^{-}(y_m + \epsilon)$ and $\mathcal{A}^{+}(y_{m+1} - \epsilon)$ are related linearly to the incoming ones. As in scattering theory we write [26]

$$\begin{aligned} \mathcal{A}^{+}(y_{m+1} - \epsilon) &= T^{+}(y_m, y_{m+1})\mathcal{A}^{+}(y_m + \epsilon) \\ &\quad + R^{-}(y_m, y_{m+1})\mathcal{A}^{-}(y_{m+1} - \epsilon), \\ \mathcal{A}^{-}(y_m + \epsilon) &= T^{-}(y_m, y_{m+1})\mathcal{A}^{-}(y_{m+1} - \epsilon) \\ &\quad + R^{+}(y_m, y_{m+1})\mathcal{A}^{+}(y_m + \epsilon) , \end{aligned} \tag{B9}$$

where the reflection and transmission matrices will be defined in the following as block diagonal matrices.

Reflection in the open interval (y_m, y_{m+1}) solely occurs in the low-velocity regime. Therefore the reflection matrix $R^{\pm}$ contains only the reflection amplitude $r^{\pm}(y_m, y_{m+1})$ taken from (B7)

$$R^{\pm}(y_m, y_{m+1}) = \begin{pmatrix} \boxed{\begin{matrix} 0 & 0 \\ 0 & r^{\pm} \end{matrix}} & & & \\ & \boxed{0} & & \\ & & \boxed{0} & \\ & & & \ddots \end{pmatrix} . \tag{B10}$$

The transition matrix $T^{\pm}$ for penetration through the

open interval (y_m, y_{m+1}) is obtained in the following block diagonal form

$$T^{\pm}(y_m, y_{m+1}) = \begin{pmatrix} \boxed{\begin{matrix} 0 & 0 \\ 0 & t^{\pm} \end{matrix}} & & & \\ & \boxed{\sigma^{\pm}_{1,2}} & & \\ & & \boxed{\sigma^{\pm}_{3,4}} & \\ & & & \ddots \end{pmatrix} . \tag{B11}$$

$t^{\pm}$ stands for the transmission amplitude $t^{\pm}(y_m, y_{m+1})$ from Eq. (B7) in the low-velocity regime. The $\sigma^{\pm}_{i,i+1}$ represent (2×2) matrices which act as propagators for the interval (y_m, y_{m+1}) in the high-velocity regime. They take account of adiabatic motion and nonadiabatic transitions at avoided crossings, which, by our definition of the intervals (y_m, y_{m+1}), are located near the middle of the interval (Fig. 4). Therefore the high-velocity propagator $s^{\pm}_{i,i+1}(y_m, y_{m+1})$ for the waves α_{n_i} and $\alpha_{n_{i+1}}$ which are coupled by an avoided crossing in y_{AC} is a product of a WKB propagator (B3), a transition matrix at y_{AC} (B5), and another WKB propagator

$$\begin{aligned} &\sigma^{+}_{i,i+1}(y_m, y_{m+1}) \\ &\quad \equiv \begin{pmatrix} c_i(y_m, y_{\mathrm{AC}}) & \\ & c_{i+1}(y_m, y_{\mathrm{AC}}) \end{pmatrix} \\ &\qquad \times s^{+}_{i,i+1}(y_{\mathrm{AC}}) \begin{pmatrix} c_i(y_{\mathrm{AC}}, y_{m+1}) & \\ & c_{i+1}(y_{\mathrm{AC}}, y_{m+1}) \end{pmatrix} . \end{aligned} \tag{B12}$$

The reverse propagator σ^{-} is given by $\sigma^{-}_{i,i+1}(y_m, y_{m+1})\sigma^{+}_{i,i+1}(y_{m+1}, y_m) = (id)$.

For the reason mentioned in [25] it is numerically untractable to proceed by constructing a total translation matrix that couples the vector at the surface $\mathcal{A}^{\pm}(0)$ to the outgoing (incoming) vector $\mathcal{A}^{\pm}(y_M)$. To facilitate the calculation, we therefore use a recursive calculation scheme which is motivated by the aforementioned analogy with the multiple reflection of a light ray in a pile of semireflective mirrors. A multichannel wave $\mathcal{A}^{[k-1]+}(y_m + \epsilon)$ penetrating through the open interval (y_m, y_{m+1}) evolves into $\mathcal{A}^{[k-1]+}(y_{m+1} - \epsilon)$. At the same time it creates a new, reflected wave $\mathcal{A}^{[k]-}(y_m + \epsilon)$ which in turn propagates back through the interval (y_{m-1}, y_m). These two (penetrating and reflected) waves create further scattered waves and so on, ad infinitum. We therefore substitute Eq. (B9) by a nonlocal recurrence relation, connecting the different generations $\mathcal{A}^{[k]}$ of reflected waves in the multilayer potential system

$$\begin{aligned} \mathcal{A}^{[k]+}(y_m - \epsilon) &= T^{+}(y_{m-1}, y_m)\mathcal{A}^{[k]+}(y_{m-1} + \epsilon) \\ &\quad + R^{-}(y_{m-1}, y_m)\mathcal{A}^{[k-1]-}(y_m - \epsilon) , \\ \mathcal{A}^{[k]-}(y_m + \epsilon) &= T^{-}(y_m, y_{m+1})\mathcal{A}^{[k]-}(y_{m+1} - \epsilon) \\ &\quad + R^{+}(y_m, y_{m+1})\mathcal{A}^{[k-1]+}(y_m + \epsilon) . \end{aligned} \tag{B13}$$

When connecting two open intervals (y_{m-1}, y_m) and (y_m, y_{m+1}) we additionally have to include a transition matrix $S^{\pm}(y_m)$ by

$$\mathcal{A}^{[k]\pm}(y_m \pm \epsilon) = S^{\pm}(y_m)\mathcal{A}^{[k]\pm}(y_m \mp \epsilon) . \tag{B14}$$

It is given as a block matrix of 2×2 transition matrices (B5) belonging to the interval boundary y_m

$$S^{\pm}(y_m) = \begin{pmatrix} 0 & & \\ & \boxed{s^{\pm}_{II,1}} & \\ & & \boxed{s^{\pm}_{2,3}} \\ & & & \ddots \end{pmatrix} . \tag{B15}$$

Using Eqs. (B9) and (B14) the wave-function vector $\mathcal{A}^{\pm}$ can now be obtained by iteratively computing its values in the points $0, y_1 \pm \epsilon, \ldots, y_{M-1} \pm \epsilon, y_M$. The iteration starts with an incoming zeroth-order wave in $y = y_M$

$$\mathcal{A}^{[0]-}_n(y_M) = \alpha^{-}_n(y_M) = \delta_{0,n} . \tag{B16}$$

This incoming wave corresponds to the incident atomic beam impinging on the prism which is per definition a pure zeroth diffraction order.

To obtain physically meaningful solutions we have to take into account reasonable boundary conditions in $y = 0$ and y_M. As we assume that atoms reaching the surface in the potentials $W_{n_i} < W_{n_{\mathrm{II}}}$ do not contribute to coherent diffraction, no reflected waves are generated in $y = 0$. In $y = y_M$ allowance is made for outgoing waves in all open channels.

The total wave function in the asymptotic region is given by summing over all amplitudes generated at iteration steps $[2l]$ (incoming) and $[2l + 1]$ (outgoing) in the point y_M

$$\Phi(y_M) = \sum_{l=0}^{\infty} \{ \mathcal{A}^{[2l]-}(y_M) + \mathcal{A}^{[2l+1]+}(y_M) \} . \tag{B17}$$

Since $y = 0$ as well as the asymptotic region, $y \geq y_M$ provide a drain for the total population in the interaction zone, the multiply reflected contributions to the reflected waves become rapidly insignificant after a few iteration cycles and the total outgoing wave-function sum (B17) converges geometrically to its final value.

To calculate the relative populations of the diffraction orders we note that an experiment would measure the particle current (probability current). This is given by the probability current density $\mathbf{j} = \frac{i\hbar}{2m}(\Phi\nabla\Phi^* - \Phi^*\nabla\Phi)$ integrated over the surface of the detector. As the current diverges for plane waves, we give the population p_n of the diffraction orders as the current of the outgoing orders normalized to the incoming current

$$p_n \equiv \frac{\int_A \mathbf{j}_{\mathrm{out},n} \cdot \mathbf{dn}}{\int_A \mathbf{j}_{\mathrm{in}} \cdot \mathbf{dn}} . \tag{B18}$$

A suitable detector surface A, containing the whole incoming and outgoing flux (cf. Fig. 1), is the (x, z) plane $y = y_M$ in the asymptotic region far from the mirror surface. Evaluation of (B18) for this surface leads to

$$p_n = \frac{p_{\infty y,n}}{p_{\infty y}} |\mathcal{A}^{+}_n(y_M)|^2 = \frac{p_{\infty y,n}}{p_{\infty y}} |\alpha_n(y_M)|^2 . \tag{B19}$$

[1] O. Carnal and J. Mlynek, Phys. Rev. Lett. **66**, 2689 (1991); D. W. Keith, C. R. Ekstrom, Q. A. Turchette, and D. E. Pritchard, *ibid.* **66**, 2693 (1991).
[2] A. P. Kazantsev, G. A. Ryabenko, G. I. Surdutovich, and V. P. Yakovlev, Phys. Rep. **129**, 75 (1985).
[3] Ph. E. Moskowitz, Ph. L. Gould, and D. E. Pritchard, J. Opt. Soc. Am. B **2**, 1784 (1985).
[4] R. J. Cook and R. K. Hill, Opt. Commun. **43**, 258 (1982).
[5] V. I. Balykin, V. S. Letokhov, Yu. B. Ovchinnikov, and A. I. Sidorov, Zh. Eksp. Teor. Fiz. **45**, 282 (1987) [JETP Lett. **45**, 353 (1987)]; Phys. Rev. Lett. **60**, 2137 (1988); M. A. Kasevich, D. S. Weiss, and S. Chu, Opt. Lett. **15**, 607 (1990).
[6] J. V. Hajnal and G. I. Opat, Opt. Commun. **71**, 119 (1989).
[7] J. V. Hajnal, K. G. H. Baldwin, P. T. H. Fisk, H.-A. Bachor, and G. I. Opat, Opt. Commun. **73**, 331 (1989).
[8] J. Dalibard and C. Cohen-Tannoudji, J. Opt. Soc. Am. B **2**, 1707 (1985).
[9] V. I. Balykin and V. S. Letokhov, Appl. Phys. B **48**, 517 (1989).
[10] H. Wallis, J. Dalibard, and C. Cohen-Tannoudji, Appl. Phys. B **54**, 407 (1992).
[11] L. D. Landau and E. M. Lifschitz, *Lehrbuch der Theoretischen Physik Band III: Quantenmechanik* (Akademie-Verlag, Berlin, 1988).
[12] E. Arimondo, A. Bambini, and S. Stenholm, Opt. Commun. **37**, 103 (1981); A. F. Bernhard and B. W. Shore, Phys. Rev. A **23**, 1290 (1981).
[13] S. Glasgow, P. Meystre, M. Wilkens, and E. M. Wright, Phys. Rev. A **43**, 2455 (1991).
[14] M. Wilkens, E. Schumacher, and P. Meystre, Phys. Rev. A **44**, 3130 (1991).
[15] This truncation is performed by limiting the indices n, n' to the interval $-N \leq n \leq N$, where N depends on the maximum Rabi frequency. The boundary N has to be chosen sufficently large to ensure that those potentials that are relevant for the further calculation converge as $N \to \infty$. For the parameter regime (grazing incidence of the atom) the number of relevant potentials is below 10 and they approach their limiting values for $N \lesssim 20$.
[16] It should be noted that the representation (3.6) of the Hamiltonian does not contain the diabatic curves as diagonal elements.
[17] C. Zener, Proc. R. Soc. London Ser. A **137**, 696 (1932); L. D. Landau, Phys. Z. Sowjetunion **2**, 46 (1932).
[18] M. S. Child, Mol. Phys. **28**, 495 (1974); J. R. Laing and T. F. George, Phys. Rev. A **16**, 1082 (1977).
[19] W. R. Thorson, J. B. Delos, and S. A. Boorstein, Phys. Rev. A **4**, 1052 (1971), and references therein.
[20] Weiping Zhang and D. F. Walls, Phys. Rev. Lett. **68**, 3287 (1992).
[21] J. Dalibard, Y. Castin, and K. Mølmer, Phys. Rev. Lett. **86**, 580 (1992).
[22] L. S. Rodberg and R. M. Thaler, *Pure and Applied Physics Vol. 26: The Quantum Theory of Scattering* (Academic, New York, 1967).
[23] I. N. Bronstein and K. A. Semendjajew, *Taschenbuch der Mathematik* (Deutsch, Thun, 1985).
[24] For an actual evaluation the numerically obtained quasipotentials are fitted to by a suitable analytic function in order to perform the integration. A natural choice for the diabatic curves $D_a(y)$, $D_b(y)$, and the coupling $C(y)$ in the region around each crossing are exponentially varying diabatic curves and a Gaussian coupling

$$D_{a,b}(y) = \frac{1}{2}\{W_{n_i}(y_{\mathrm{AC}}) + W_{n_{i+1}}(y_{\mathrm{AC}})\} \pm d_1\{\exp[-d_2(y - y_{\mathrm{AC}})] - 1\}$$
$$C(y) = c_1 \exp\{-c_2(y - y_{\mathrm{AC}})^2\} .$$

The upper sign refers to to the index a. Thus the local analytic expression for the adiabatic potential is

$$W_{n_{i/i+1}} = \tfrac{1}{2}\{W_{n_i}(y_{\mathrm{AC}}) + W_{n_{i+1}}(y_{\mathrm{AC}})\} \pm \sqrt{D_a^2(y) + C^2(y)}.$$

The upper sign refers to the index i so that $W_{n_i} > W_{n_{i+1}}$. From the fitted analytic expression the complex intersection points (in general more than one) are iterated as the roots of the equation $W_{n_i} = W_{n_{i+1}}$. As a good approximation one picks up only the contribution of the intersection point that is nearest to the real axis.
[25] Equation (B7) defines a scattering matrix for waves in the two open channels for each open interval (y_m, y_{m+1}) in the low-velocity regime. In analogy to the high-velocity regime it might seem appropriate to work with a translation matrix that maps the amplitudes of incoming and outgoing waves from y_m to y_{m+1}. As one knows from the example of penetration through a thick barrier, the amplitudes of such a translator are generally not bound in absolute value. This would cause numerical breakdown in the further calculation. On the contrary the transmission and reflection amplitudes are bound corresponding to their physical meaning.
[26] In analogy to (B7) the four matrices $T^{\pm}$ and $R^{\pm}$ can be visualized as four blocks of a scattering matrix that maps the incoming waves in all open channels of the open interval (y_m, y_{m+1}) on the outgoing waves.